High-payload and agile hopping leg prototype

Giorgio Valsecchi and Marco Hutter

***Abstract*— This paper presents the design and experimental evaluations of an articulated robotic leg. The main scope of this new design is to combine high payload capabilities with agile locomotion. While both high payloads and agility have been achieved individually by different walking robots, designs intended for both have not been proposed yet. We optimized pseudo-direct-drive actuators to provide high torques density while simultaneously having good efficiency, low heat generation, and sufficient velocity to address the challenge. A two-DOF leg prototype has been designed and manufactured. The experimental test setup for the leg prototype is explained, and the results of the first hopping experiments are reported.**

***Paper Type* – Original Work**

I. INTRODUCTION

Compared to tracked or wheeled vehicles, legged robots have advantages, particularly in terms of mobility and versatility. Significant advances over the recent years demonstrated the viability of walking robots in multiple scenarios. Currently, quadrupedal robots are commercially available [1], [2], [3], and can be successfully employed in complex missions, like the DARPA Subterranean (SubT) Challenge [4], [5], [6].

Despite all the recent positive developments, legged robots still cannot match the versatility of biological systems. Dogs and horses can carry significant masses over challenging terrains, indoor and outdoor, for hours, without overheating and without frequent recharges, or carry a larger load for a short time.

Boston Dynamics' big dog [7] and LS3 [8] achieved a payload of 90 kg and a range of 32 km, while HyQReal managed to tow a 3300 kg aircraft [9]. Unfortunately, hydraulic actuation and ICEs are not compatible with all applications. Exhaust gas prevents robots from operating indoors, and the possibility of hydraulic oil jets and leakages [10] is a strong reason not to deploy these systems near non-expert users and humans in general.

Fully electric robots are much more suitable for operating indoors and near humans, but their performance is limited. Spot and ANYmal have both payloads of $\sim$12 Kg for robot masses of $\sim$40 Kg and a runtime of 90 minutes (without payload), corresponding to an autonomy below 10 Km [3][1]. Research platforms perform similarly; IIT Centauro [11] and DFKI SpaceClimber [12] showed higher payloads at the cost of using static gaits and lower velocities. MIT's Cheetah 3 [13], and JPL's LLAMA [14] perform well from a velocity point of view but did not demonstrate a higher payload.

This work was supported by ESA Contract Number 4000131516/20/NL/MH/ic.

All authors are with the Robotic Systems Lab (RSL), ETH Zürich, Switzerland. vgiorgio@ethz.ch

Fig. 1: Robotic leg prototype mounted on a linear guide.

Smaller robots, on the other hand, show better payload-to-weight ratios, also because of advantageous scaling laws of physics [15], [16], [17]. MIT Mini cheetah [18] and SOLO [19] are good examples, with the mini cheetah reaching a payload close to its weight.

This work introduces a newly developed electrically actuated robotic leg aiming to achieve large payloads and agile locomotion. The paper is organized as follows: Sec. II introduces the kinematics and design of the leg prototype accompanied by details on the experimental setup, Sec. III presents results results from preliminary trials, and Sec. IV addresses the conclusions and comments on future work.

II. SYSTEM DESCRIPTION

The robotic leg prototype, shown in fig.1,is composed of two actuated degrees of freedom: hip flexion/extension (HFE) and knee flexion/extension (KFE). The joints are arranged in serial configuration for energetic reasons to avoid antagonistic power [23]. We built the HFE actuator combining a brushless DC motor with an integrated custom-built planetary gearbox. We used the same motor with a balls-crew (THK-SDA1530V) and linkage transmission for

TABLE I: Motor performance

Motor	Peak torque [Nm]	Motor constant [Nm/W$^{0.5}$]	Weight [kg]
REVO1-30 [20]	40	0.818	1.0
ILM 115x25 [21]	12.7	0.88	1.2
LSI-160 [14]	42.5	0.644	2.1
HT05001 [22]	21.3	0.43	1.3

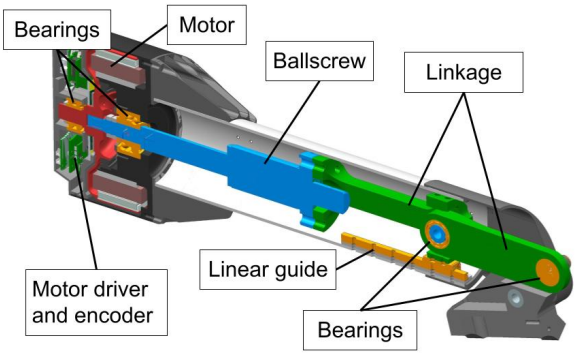

Fig. 2: Cross-section of the thigh showing the integrated transmission. The rotor (red) is connected to the ball-screw (blue) that drives the linkage (green), bringing the motion to the knee axis.

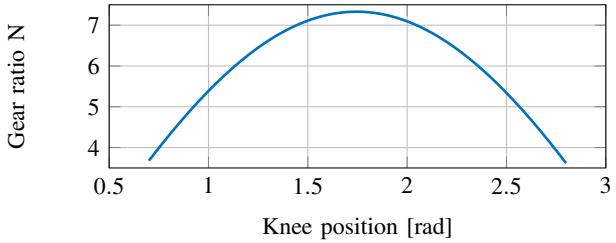

Fig. 3: Plot of the knee transmission ratio as a function of the knee angle θ_{KFE}.

the KFE to remove mass from the knee and minimize inertia. The motors are controlled by ANYdrive motor-driver and RLS off-axis magnetic encoders. Fig. 2 shows a cross-section of the thigh and knee actuator.

We selected the motor with the biggest motor constant K_m and torque density. Table I shows how the selected REVO1-30 motor stands out compared to other motors used for similar applications. Winding losses P_h are proportional to the squared of the motor torque τ_m, which is connected to the joint torque τ_j via the gear ration N, according to eq. 1.

$$P_h = \left(\frac{\tau_m}{K_m}\right)^2 = \left(\frac{\tau_j}{K_m N}\right)^2 \tag{1}$$

Therefore we selected the highest gear ratio possible to minimize heat production. This resulted in a gear ratio of 4.13 for the HFE. The linkage of the KFE introduces a variable gear ratio, as shown in fig. 3, that ranges between 5 and 7 for the portion of ROM used during walking.

Both the thigh and the shank have a length of 0.33 m, and overall the leg weights 5.7 kg. A standard ANYmal C foot was used as a contact element.

We mounted the leg on a linear guide for the experiments, as shown in fig. 1. A virtual model controller emulating a spring between the HFE actuator and the ground is used when the foot is in contact, while an inverse dynamic controller is used during the flight phase [21].

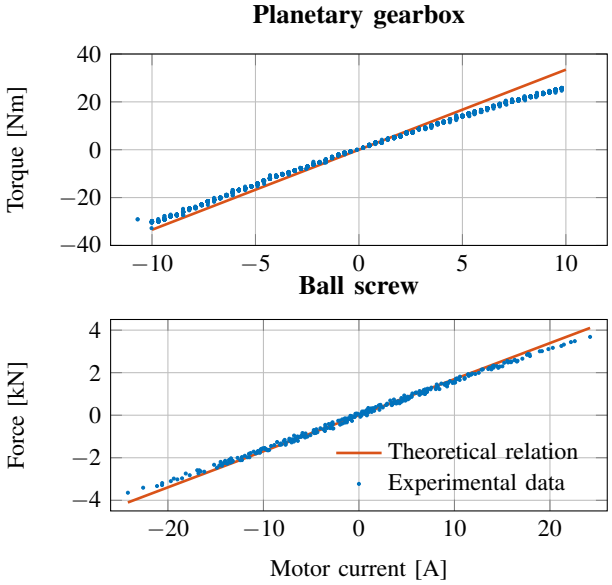

Fig. 4: Experimental characterisation of the planetary gearbox and ball screw actuators compared with the expected theoretical behaviors.

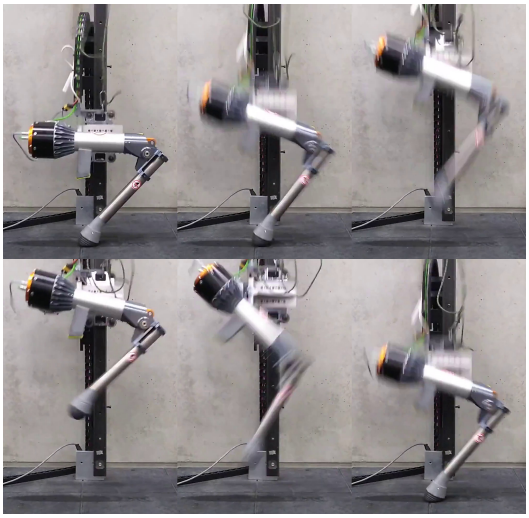

Fig. 5: Picture sequence of the leg prototype mounted on a vertical rail, performing a vertical jump. Time between two frames: 0.1 seconds.

III. RESULTS

To validate the performance of the newly developed actuators, we performed an experimental characterization. We connected the output of the actuators (the moving nut for the linear drive) to a six-axis force/torque sensor and commanded arbitrary motor currents. Fig. 4 shows how the experiments are consistent with what would be predicted just by the gear ratio and torque constant of the motor. Friction, stick-slip, and hysteresis can explain the minor deviations from linearity and data dispersion.

The first series of experiments have been made with the entire leg prototype using the experimental setup as explained

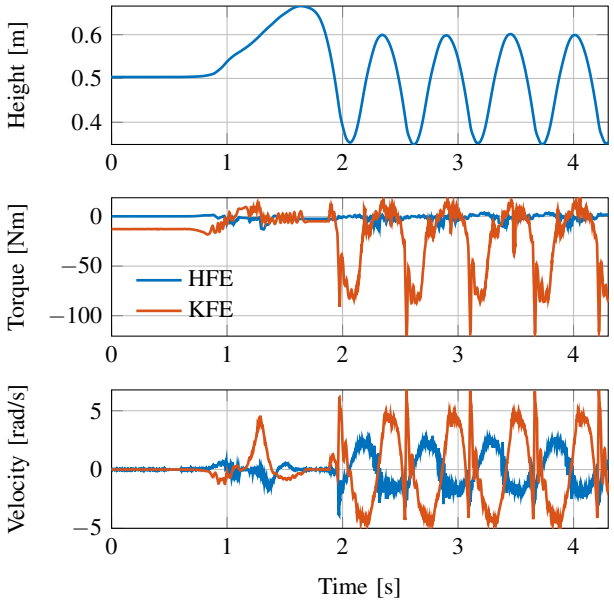

Fig. 6: Base height, joint torques and velocities during an hopping experiment. The base is first lifted and then dropped, first touch-down is at second 2. Four distinct hops are visible between seconds 2 and 4.

in the previous section. We performed all tests with a voltage of 48V, provided by an external power supply. The system has been tuned, and basic reference tracking tests have been performed both in joint and task space, first with the leg suspended and then with the foot in contact with the ground.

We controlled a continuous hopping motion to test the leg's dynamic performance. The virtual spring-damper was tuned to such motion [21]. A picture sequence of the hopping is shown in fig. 5. The leg can reach a vertical velocity of 2.3 m/s and a height comparable with its size. The hopping motion can be sustained continuously with 50 W total average winding losses, reaching an equilibrium temperature of 40 deg C, measured at the motor housing, in 1 h. We obtained similar results with additional 10 kg attached to the rail slider.

Fig. 6 illustrates the behavior of the leg during a hopping experiment. Initially, the leg is motionless and in contact with the ground; the standing torques are visible. Then it is lifted to 0.65 m and dropped. The touchdown is visible as a spike in velocity at second 2. Four hops are executed after second 2, characterized by alternating velocities for both the actuators and significantly larger torques for the KFE actuator. Currents are not shown because they are directly proportional to toques, as shown in fig. 4. Torque and velocity ripples caused by cogging are also visible in the plots.

Fig. 7 gives a qualitative measure of the strength achieved by the leg prototype. Sustaining a 65 kg person requires 140 Nm, at the KFE joint, only half of what the actuator can provide. However, this is more than its nominal torque (around 70 Nm) and can be sustained only for a limited amount of time, in the order of 20 s, before overheating.

Fig. 7: Leg prototype sustaining a 65 kg person.

IV. CONCLUSIONS

Some of the issues regarding the design of the leg and the future improvements are reported next.

The prototype's points of improvement can be grouped into two distinct categories. Firstly, the performance limiting ones. In this category, the main design challenge is matching the gear ratio and motor's velocity constant. The gear ratio in the current prototype is limited by geometrical factors, commercial components, and design unknowns leading to big safety factors. With custom components, the gear ratio could be increased and heat generation reduced. On the other hand, the motor's velocity constant should be adjusted to satisfy the speed requirements. However, changing the velocity constant requires custom motor windings representing a big manufacturing challenge. The actuator's strong magnets, high-transparency transmission, and low inertia links result in large cogging torques. A proper cogging compensation strategy is necessary to minimize velocity ripples. Another possible improvement is the sizing of the HFE actuator. As can be seen in fig. 6 very little torque is actually required for this motion. Further analysis and simulation should evaluate the possibility of using a smaller motor and reducing weight. Finally, the ANYdrive's motor drivers have oversized microcontrollers for this task, resulting in high idling power consumption. The second group consists of details that make the prototype challenging to operate or maintain and impractical for a complete quadruped. Examples are the lack of joint output encoders, which require zeroing the leg at startup, and hard to disassemble parts.

Despite the improvable aspects mentioned above, the prototype successfully demonstrated the possibility of building an electrically actuated robotic leg that combines high payload and agile motions. Future steps include more hardware experiments, simulations, and design iterations. The final goal of this project is to optimize the proposed design for a full-scale quadruped robot.

REFERENCES

[1] "Spot." [Online]. Available: https://www.bostondynamics.com/spot

[2] "Aliengo." [Online]. Available: https://www.unitree.com/products/aliengo

[3] "Anymal - autonomous legged robot," May 2021. [Online]. Available: https://www.anybotics.com/anymal-autonomous-legged-robot/

[4] M. Tranzatto, "Cerberus: Autonomous legged and aerial robotic exploration in the tunnel and urban circuits of the darpa subterranean challenge," *Journal of field robotics.*, 2021.

[5] A. Bouman, M. F. Ginting, N. Alatur, M. Palieri, D. D. Fan, T. Touma, T. Pailevanian, S.-K. Kim, K. Otsu, J. Burdick, *et al.*, "Autonomous spot: Long-range autonomous exploration of extreme environments with legged locomotion," in *2020 IEEE/RSJ International Conference on Intelligent Robots and Systems (IROS)*. IEEE, 2020, pp. 2518–2525.

[6] I. D. Miller, F. Cladera, A. Cowley, S. S. Shivakumar, E. S. Lee, L. Jarin-Lipschitz, A. Bhat, N. Rodrigues, A. Zhou, A. Cohen, *et al.*, "Mine tunnel exploration using multiple quadrupedal robots," *IEEE Robotics and Automation Letters*, vol. 5, no. 2, pp. 2840–2847, 2020.

[7] M. Raibert, K. Blankespoor, G. Nelson, and R. Playter, "Bigdog, the rough-terrain quadruped robot," *IFAC Proceedings Volumes*, vol. 41, no. 2, pp. 10 822–10 825, 2008, 17th IFAC World Congress. [Online]. Available: https://www.sciencedirect.com/science/article/pii/S1474667016407020

[8] BostonDynamics, "Ls3 - legged squad support system," Sep 2012. [Online]. Available: https://youtu.be/R7ezXBEBE6U

[9] C. Semini, V. Barasuol, J. Goldsmith, M. Frigerio, M. Focchi, Y. Gao, and D. G. Caldwell, "Design of the hydraulically actuated, torque-controlled quadruped robot hyq2max," *IEEE/ASME Transactions on Mechatronics*, vol. 22, no. 2, pp. 635–646, April 2017.

[10] "Inside the lab: How does atlas work?" Aug 2021. [Online]. Available: https://youtu.be/EezdinoG4mk?t=120

[11] N. Kashiri, L. Baccelliere, L. Muratore, A. Laurenzi, Z. Ren, E. M. Hoffman, M. Kamedula, G. F. Rigano, J. Malzahn, S. Cordasco, *et al.*, "Centauro: A hybrid locomotion and high power resilient manipulation platform," *IEEE Robotics and Automation Letters*, vol. 4, no. 2, pp. 1595–1602, 2019.

[12] S. Bartsch, T. Birnschein, M. Römmermann, J. Hilljegerdes, D. Kühn, and F. Kirchner, "Development of the six-legged walking and climbing robot spaceclimber," *Journal of Field Robotics*, vol. 29, no. 3, pp. 506–532, 2012.

[13] G. Bledt, M. J. Powell, B. Katz, J. Di Carlo, P. M. Wensing, and S. Kim, "Mit cheetah 3: Design and control of a robust, dynamic quadruped robot," in *2018 IEEE/RSJ International Conference on Intelligent Robots and Systems (IROS)*. IEEE, 2018, pp. 2245–2252.

[14] J. Nicholson, J. Jasper, A. Kourchians, G. McCutcheon, M. Austin, M. Gonzalez, J. Pusey, S. Karumanchi, C. Hubicki, and J. Clark, "Llama: Design and control of an omnidirectional human mission scale quadrupedal robot," in *2020 IEEE/RSJ International Conference on Intelligent Robots and Systems (IROS)*. IEEE, 2020, pp. 3951–3958.

[15] M. Wautelet, "Scaling laws in the macro-, micro- and nanoworlds," *European Journal of Physics*, vol. 22, no. 6, pp. 601–611, oct 2001. [Online]. Available: https://doi.org/10.1088%2F0143-0807%2F22%2F6%2F305

[16] P. M. Wensing, A. Wang, S. Seok, D. Otten, J. Lang, and S. Kim, "Proprioceptive actuator design in the mit cheetah: Impact mitigation and high-bandwidth physical interaction for dynamic legged robots," *Ieee transactions on robotics*, vol. 33, no. 3, pp. 509–522, 2017.

[17] K. J. Waldron and C. Hubert, "Scaling of robotic mechanisms," in *Proceedings 2000 ICRA. Millennium Conference. IEEE International Conference on Robotics and Automation. Symposia Proceedings (Cat. No. 00CH37065)*, vol. 1. IEEE, 2000, pp. 40–45.

[18] B. K. et al., "Mini cheetah: A platform for pushing the limits of dynamic quadruped control," in *2019 International Conference on Robotics and Automation (ICRA)*, May 2019, pp. 6295–6301.

[19] F. Grimminger, A. Meduri, M. Khadiv, J. Viereck, M. Wüthrich, M. Naveau, V. Berenz, S. Heim, F. Widmaier, T. Flayols, J. Fiene, A. Badri-Spröwitz, and L. Righetti, "An open torque-controlled modular robot architecture for legged locomotion research," *IEEE Robotics and Automation Letters*, vol. 5, no. 2, pp. 3650–3657, 2020.

[20] P. Nguyen and B. Ø. Børnich, "Human-like direct drive robot," Mar. 12 2020, uS Patent App. 16/485,635.

[21] J. Hwangbo, V. Tsounis, H. Kolvenbach, and M. Hutter, "Cable-driven actuation for highly dynamic robotic systems," in *2018 IEEE/RSJ International Conference on Intelligent Robots and Systems (IROS)*, 2018, pp. 8543–8550.

[22] S. Seok, A. Wang, M. Y. Chuah, D. Otten, J. Lang, and S. Kim, "Design principles for highly efficient quadrupeds and implementation on the mit cheetah robot," in *2013 IEEE International Conference on Robotics and Automation*, 2013, pp. 3307–3312.

[23] A. Abate, J. W. Hurst, and R. L. Hatton, "Mechanical antagonism in legged robots." in *Robotics: Science and Systems*, vol. 6. Ann Arbor, MI, 2016.